Engineering Geology 292 (2021) 106248

Contents lists available at ScienceDirect

Engineering Geology

journal homepage: www.elsevier.com/locate/enggeo

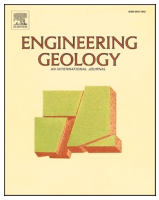

Regional-scale simulation of flowslide triggering in stratified deposits

Xiang Li, José J. Lizárraga, Giuseppe Buscarnera *

Northwestern University, Department of Civil and Environmental Engineering, United States of America

ARTICLE INFO

Keywords:
Flowslides
Spatial heterogeneity
Transient infiltration
Spatially distributed model

ABSTRACT

Capturing the failure mechanisms responsible for static liquefaction is a challenging task for the zoning of landslide susceptibility. While geomechanical models accounting for solid-fluid coupling can identify locations prone to flowslides, their performance in regional settings is impacted by the lack of procedures to replicate accurately stratigraphic heterogeneities. To mitigate this inconvenience, this paper discusses the performance of a spatially-distributed model aimed at capturing distinct landslide triggering mechanisms in layered deposits. The model relies on the simultaneous computation of multiple factors of safety associated with the triggering of frictional slips and liquefaction-induced flowslides. In addition, the spatiotemporal variation of such indices is retrieved from a vectorized finite element platform solving pore pressure transients in stratified unsaturated soils. Such features enable the model to take into account the vertical heterogeneity of individual slope units, while dramatically reducing the computational cost of regional-scale analyses. For illustrative purposes, the model is used to analyze a series of documented shallow landslides that occurred in Campania (Italy) following heavy rainstorms. A comparison of model predictions with and without stratigraphic heterogeneity is provided, showing that the incorporation of site heterogeneity leads to a substantial improvement of the model's spatio-temporal performance, as well as of its ability to identify different modes of failure. Furthermore, the model is applied to four municipalities across the region of interest, each characterized by different representative stratigraphic settings. Despite some mismatches, often linked to the scarcity of site-specific information, the numerical results obtained on the basis of the available dataset shows that the proposed methodology is a robust and effective tool for landslide susceptibility mapping in stratified deposits.

1. Introduction

Landslide susceptibility zonation is the first step of regional hazard management (Ayalew and Yamagishi, 2005). Very often, it is also an extraordinarily challenging task, especially in case of rainfall induced slope instabilities, which can take place within a temporal interval of few hours and involve areas of several km^2 (Baum et al., 2005; Van Westen et al., 2006). More importantly, various failure modes (Hungr et al., 2014) can exist across the same landscape, each leading to a different degree of post-failure mobility. Among them, two interesting end-members are frictional slips (characterized by a clearly identifiable failure surface and often displaying slow, episodic movement) and liquefaction-induced flowslides (caused by an unstable growth of the pore fluid pressure and ensuing rapid runaway movements). Such different forms of shallow landslides can often be observed within same region (Cascini et al., 2008), depending on site-specific combinations of slope angle, porosity and degree of saturation (Picarelli et al., 2008; McKenna et al., 2012). As a result, their complexity and coexistence call for an accurate characterization of the underlying hydro-mechanical processes responsible for the initiation of either form of slope failure. Over the last several decades, a remarkable amount of contributions to the regional-scale modeling of landslide models has become available (Montgomery and Dietrich, 1994; Wu and Sidle, 1995; Pack et al., 1998; Crosta and Frattini, 2003; Baum et al., 2010; Bellugi et al., 2015), most of them being rooted on the mechanics of frictional failure. However, comparatively smaller attention has been given to shallow landslides driven by other forms of soil instability, such as static liquefaction.

A departure from such logic is encoded into recently proposed numerical strategies to compute safety factors for flowslide triggering at regional scale (Lizárraga and Buscarnera, 2017; Lizárraga and Buscarnera, 2017). Similar to earlier suggestions (Iverson and Major, 1987; Iverson, 2005; Buscarnera and Di Prisco, 2013), these tools capture the role of hydro-mechanical coupling on the onset of shallow landslides. However, they also make reference to the idealized case of

* Corresponding author.
E-mail address: g-buscarnera@northwestern.edu (G. Buscarnera).

https://doi.org/10.1016/j.enggeo.2021.106248
Received 22 November 2020; Received in revised form 18 June 2021; Accepted 23 June 2021
Available online 25 June 2021

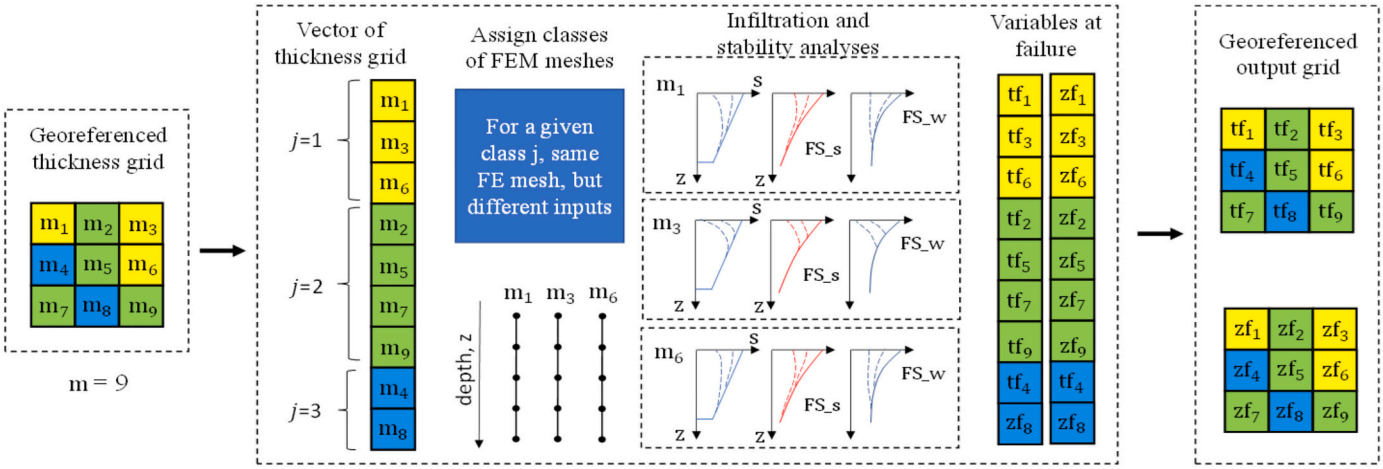

Fig. 1. Schematic representation of model workflow: m = number of cells, j = number of cell classes with the same FE mesh, tf = failure time, zf = failure depth, s = suction, FS_s = factor of safety of slips failure; FS_w = factor of safety of flowslides.

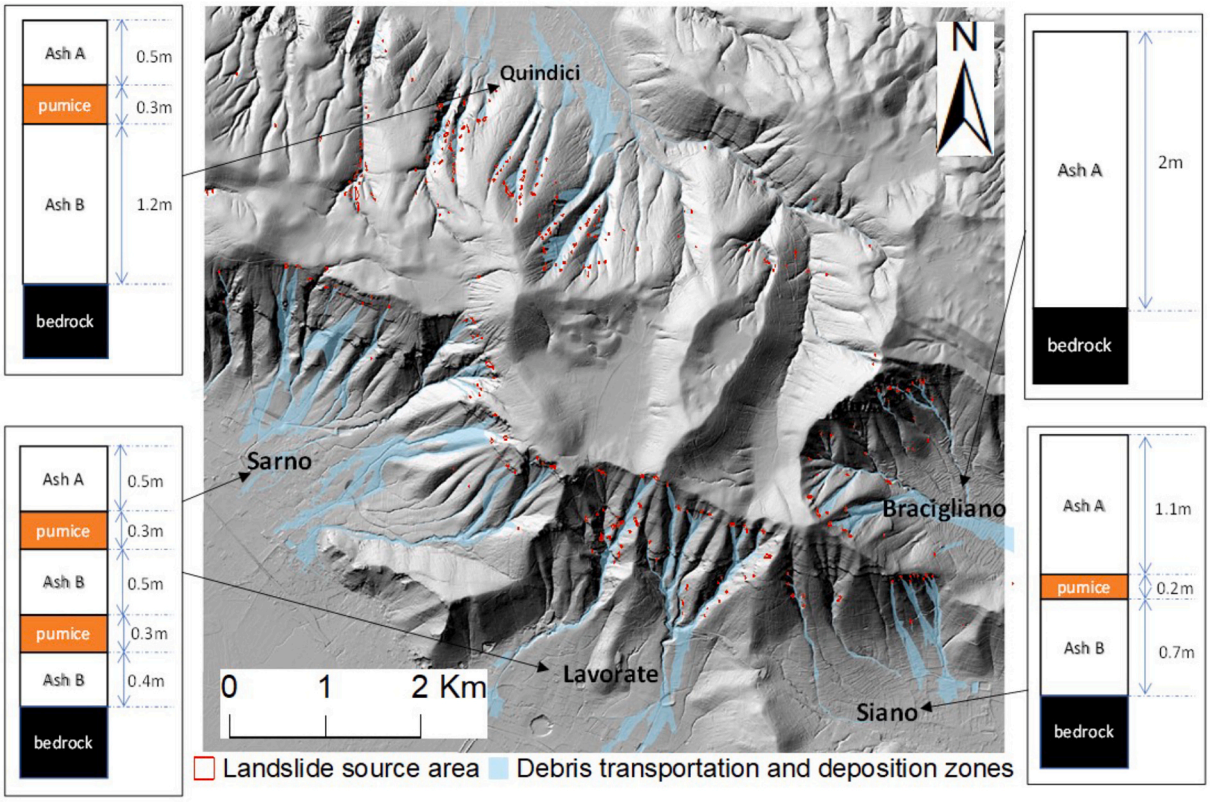

Fig. 2. Stratigraphic conditions for multiple sites across a portion of the Pizzo d'Alvano massif affected by shallow landslides and failure source area (based on Crosta and Dal Negro, 2003; Cascini and Sorbino, 2003).

homogeneous deposit, which is widely known to affect severely the intensity of pore pressure transients, the location of failure zones and the degree of saturation at failure (Cuomo and Iervolino, 2016; Reid, 1997; De Vita et al., 2013).

This paper aims to remove the abovementioned approximations in the representation of the natural heterogeneity by incorporating stratigraphic layering in the analysis of flowslide triggering. The main goal of the analyses is to explore how permeability and strength contrasts between layers can either promote or hinder the initiation of liquefaction-induced failure. For this purpose, the methodology proposed hereafter builds on the vectorized Finite Element framework recently proposed by Lizárraga and Buscarnera (2018), through which it is possible to solve transient infiltration equations in regional-scale settings in a computationally efficient fashion. The following sections illustrate briefly the numerical model and its implementation. Afterwards, the model is tested with reference to an extensively studied series of shallow landslides that took place in 1998 in the region of Campania, Italy, after a heavy rainstorm event (Crosta and Dal Negro, 2003; Di Crescenzo and Santo, 2005; Guadagno et al., 2005). Finally, the same methodology is used with reference to four municipalities characterized by different representative stratigraphic conditions, in order to discuss its performance in the presence of sites with widely different site heterogeneity.

Table 1
Description of mechanical parameters and calibrated values.

Name of parameter (units)	Symbol	Calibrated value
Friction angle (°)	ϕ'	38
Mobilized friction angle at the onset of static liquefaction (°)	ϕ^{LIQ}	26
Suction-sensitivity of shear strength (−)	k	0.6
Plastic compressibility (−)	λ	0.11
Suction-hardening parameter Ash A (Kpa^{-1})	r_w (Ash A)	7.35
Suction-hardening parameter Ash B (Kpa^{-1})	r_w (Ash B)	0.72
Suction-hardening parameter Pumice (Kpa^{-1})	r_w (Pumice)	0.0

2. Model implementation

2.1. Hydraulic model

A key component involved in the analysis of rainfall-induced landslide processes is the simulation of pore pressure transients due to infiltration events. Such steps relies on the enforcement of the water mass balance, which in the unsaturated regime can expressed as follows (Richards, 1931):

$$nC_w(h)\frac{\partial h}{\partial t} = \nabla\cdot[K(h)\nabla(h+z)] \quad (1)$$

where n is the porosity, h is the pressure head induced by capillarity, t is time, z is the vertical coordinate, $K(h)$ is a hydraulic conductivity function (HCF), and $C_w(h)$ is the unsaturated storage coefficient (i.e., the rate of change of degree of saturation S_r, with respect to h, determined by water retention curve, WRC). Eq. (1) supplemented with initial and boundary conditions constitute the problem to solve for each slope unit within the landscape.

Although under special circumstances such second-order partial differential equation can be solved in analytical form (Iverson, 2000; Srivastava and Yeh, 1991), the wide variety of nonlinear models for water retention and permeability, as well as the need to incorporate natural heterogeneity, often call for numerical solutions. Here, a Finite Element algorithm is used for this purpose (Lizárraga and Buscarnera, 2018) in order to ensure flexible assignation of material properties, boundary conditions and layering characteristics. This choice involves a spatiotemporal discretization in order to convert the differential problem in algebraic form (Celia et al., 1990; Van Dam and Feddes, 2000). Galerkin spatial discretization and an explicit forward temporal scheme

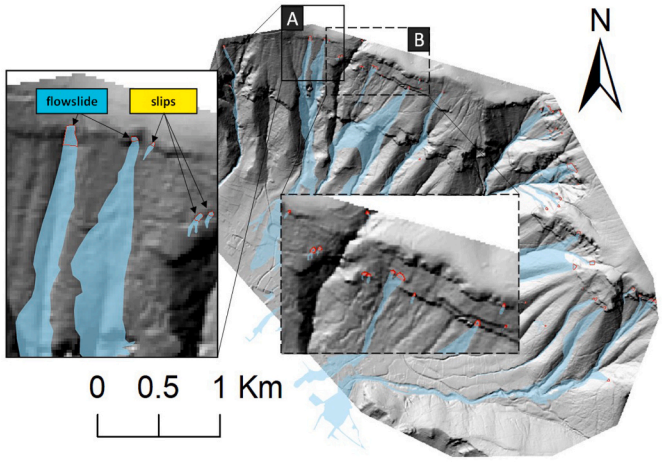

Fig. 4. Landslide transportation and deposition zones (Crosta and Dal Negro, 2003).

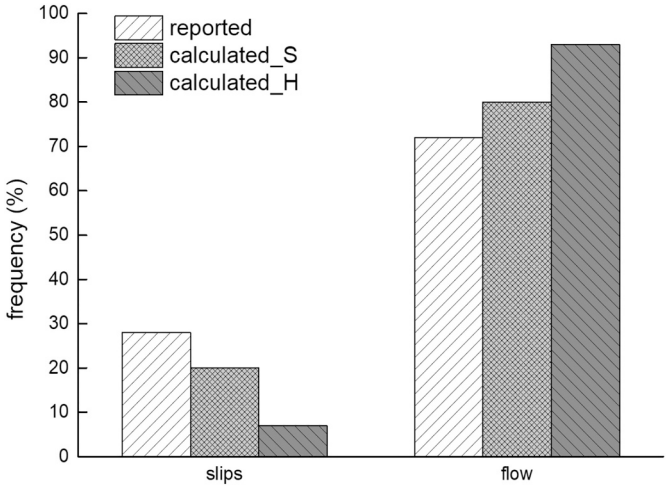

Fig. 5. Reported and computed relative frequency of slope failure mechanisms.

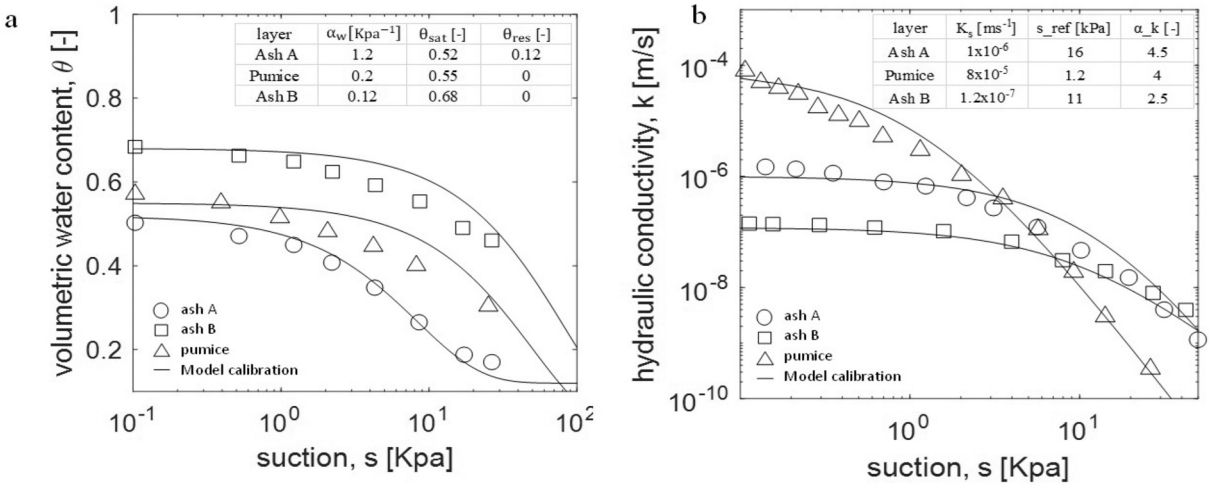

Fig. 3. Calibration of hydraulic parameters: a) water retention curve (data after Crosta and Dal Negro, 2003), b) hydraulic conductivity function (data after Pirone et al., 2015).

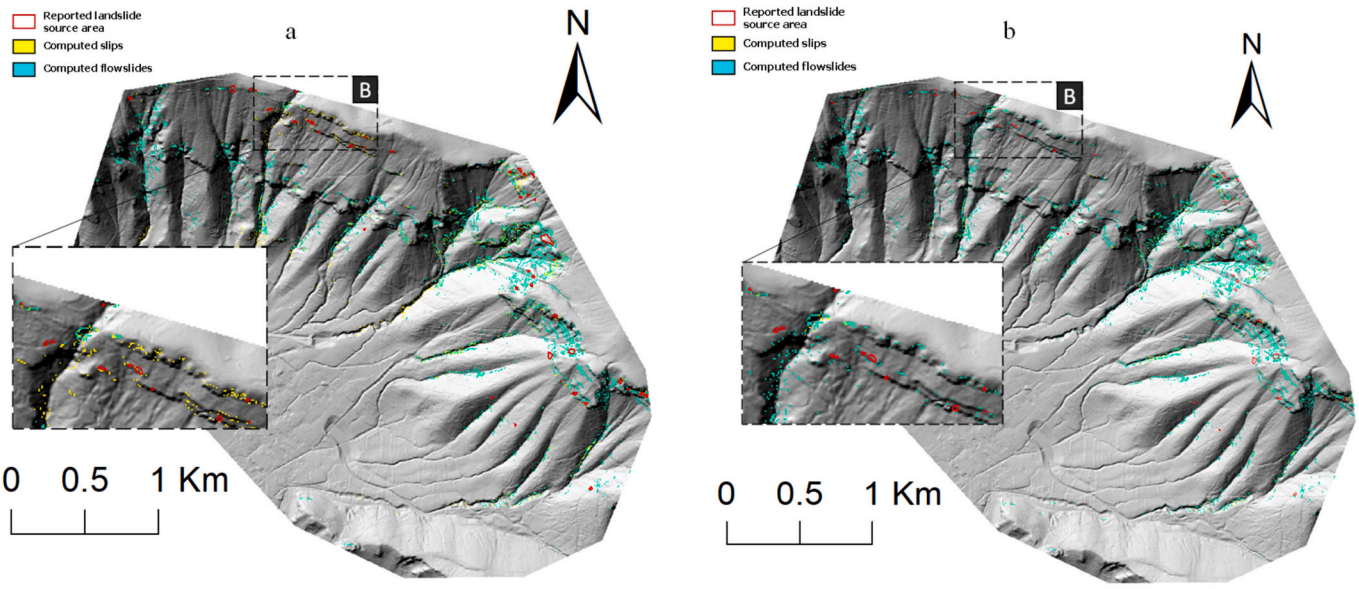

Fig. 6. Spatial distribution of simulated failure mechanisms through a) model based on layered slopes, b) model based on homogeneous slopes.

Table 2
Comparison of performance metrics from models with homogeneous and layered slopes. The simulations based on homogeneous slopes assume constant saturated permeability throughout the domain, with value equal to that Ash A. For the stratified model, the Table indicates only the value of saturated permeability, k_s, of Ash A. The value of k_s for the other layers is defined in accordance with the hydraulic parameter calibration illustrated in Fig. 3.

Homogeneous model	SI (%)	SI/EI	Stratified model	SI (%)	SI/EI
$K_s = 1 \times 10^{-6}$ m/s	12.7	12	$K_s = 1 \times 10^{-6}$ m/s	18	12
$K_s = 2 \times 10^{-6}$ m/s	28.3	12	$K_s = 2 \times 10^{-6}$ m/s	30	12.5
$K_s = 3 \times 10^{-6}$ m/s	23.8	12	$K_s = 3 \times 10^{-6}$ m/s	33.6	12.4

have been used, thus following standard computational techniques for multi-phase flow (Chen et al., 2006; Zienkiewicz et al., 1999).

2.2. Mechanical model

Landslide susceptibility analyses require the evaluation of the margin of safety of individual slope units. Here, such step is carried out with reference to idealized infinite slope models spatially distributed across the landscape. For each of these, factors of safety, FS, are computed in order to signal failure (i.e., FS < 1, in accordance with standard limit equilibrium methods; Duncan et al., 2014). In this paper, the FS expressions proposed by Lizárraga and Buscarnera (2017) on the basis of material stability theories (Buscarnera and Di Prisco, 2011; Buscarnera and Di Prisco, 2012) have been used to assess instabilities initiated by either frictional slip or liquefaction (i.e., flowslides). Specifically, the FS associated with the onset of frictional slips under drained conditions is given by:

$$FS_{SLIPS} = \frac{tan\phi'}{tan\alpha}\chi_s \tag{2a}$$

$$\chi_s = 1 + \frac{ks}{\sigma^{net}} \tag{2b}$$

where ϕ' and α are friction angle and slope inclination, respectively, σ^{net} is the net stress, s is the suction value and k is a parameter that quantifies the effect of suction on the shearing resistance. The coefficient χ_s incorporates the effect of suction on stability of the slope, reflects the suction variation impact on strength. By contrast, the FS reflecting the onset of flowslides is given by:

$$FS_{FLOWS} = \frac{tan\phi^{LIQ}}{tan\alpha}\chi_s\chi_w \tag{3a}$$

$$\chi_w = 1 - \left(\frac{\sigma^{net}}{k}\right)\left(r_w + \frac{n}{\lambda S_r G(S_r)}\right) \tag{3b}$$

where ϕ^{LIQ} is the mobilized friction angle at the onset of liquefaction, r_w is a suction-hardening parameter, λ is the plastic compressibility, S_r is the degree of saturation, $G(S_r)$ is the derivative of the water retention curve with respect of S_r. As is readily apparent from the previous expressions, both types of FS are expressed as functions of suction, thus incorporating a strong dependence of the margins of safety on transient hydraulic processes.

2.3. Vectorized Finite Element framework

The vectorized Finite Element framework used in this paper was proposed by Lizárraga and Buscarnera (2018). Rather than simulating sequentially infiltration equations for all the cells of a discretized landscape, this method runs the calculations in aggregated form by arranging the cells representing individual slope units through a matrix notation. The main benefit of such strategy is the possibility to substantially reduce the computational costs of a regional-scale analyses. For example, with reference to the computational assessment of landslide susceptibility for an 8 km^2 landscape discretized with pixel resolution of 5 × 5 m, this approach can result to computation time of about one third compared to a sequential solution method. The key features of the vectorization algorithm specific for this paper are schematically depicted in Fig. 1, while further details are provided by Lizárraga and Buscarnera (2018).

3. Case study

3.1. Selected site

The events that took place in 1998 in Campania, Italy, after a heavy rainstorm, represent some of the most extensively studied cases of shallow landslide of the recent history. Detailed accounts of these events are provided by numerous contributions (Crosta and Dal Negro, 2003; Guadagno et al., 2005; Cascini et al., 2011). Here, only key data immediately relevant for the purposes of this paper are briefly discussed.

The area of interest is in the Pizzo d'Alvano massif. The soils involved in the abovementioned shallow landslides consistent of interbedded

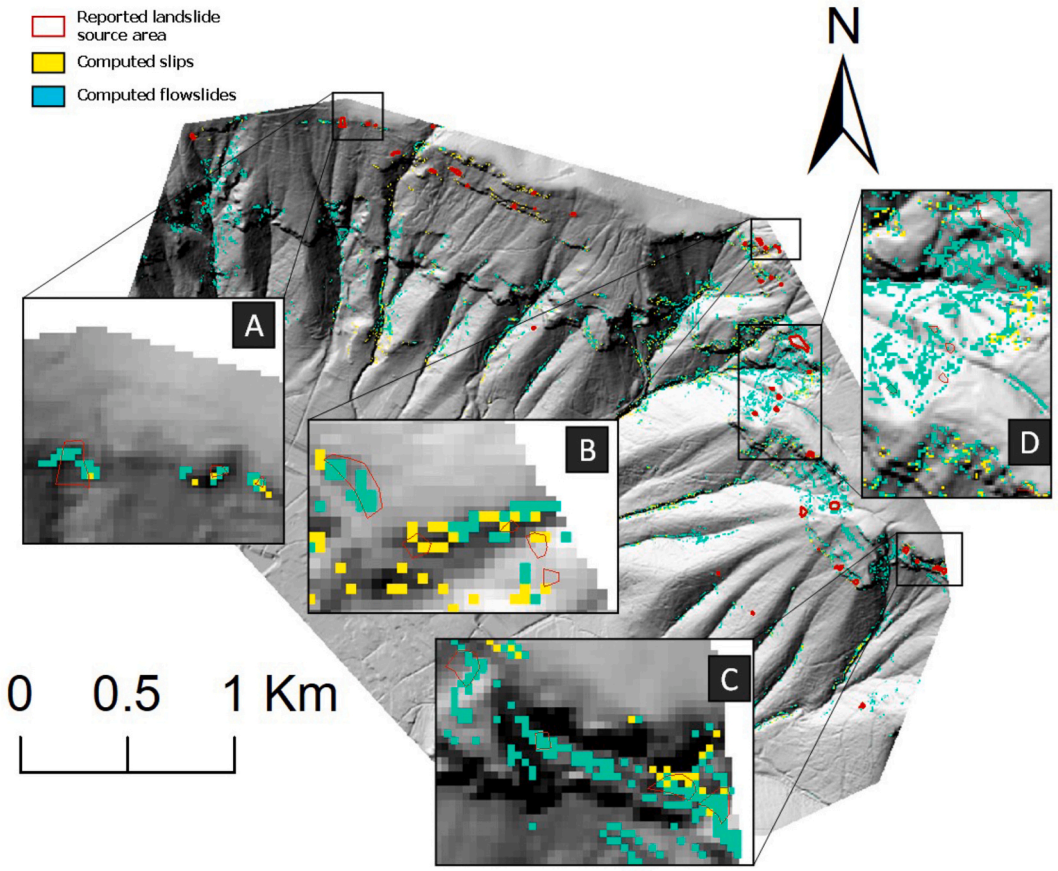

Fig. 7. Predicted landslide triggering mechanisms in the Sarno site (source areas reported by Frattini et al., 2004).

layers of unconsolidated air-fall pyroclastic deposits. Here, alternations of ashes and pumices are often found, resulting in stratified profiles across the landscape (Cascini et al., 2005) with thickness ranging from less than a meter to more than 5 m (Cascini et al., 2008). While the landscapes where most landslides occurred are characterized by a depth to bedrock within 2 m. In such accordance, computation in this work involved slope units are with thickness of 0.5 m, 1.3 m and 2 m. Furthermore, the hydrologic properties of ashes vary according to their deposition history and depth (Sorbino and Nicotera, 2013). As a consequence, two types of ash, labeled as A and B (for the upper and buried ashes, respectively) are defined.

Although highly variable layering was found across the region, Crosta and Dal Negro (2003); Cascini and Sorbino (2003) identified typical stratigraphic profiles for multiple sites across the affected area (Fig. 2). At the same time, the landslides source areas were mapped over the landscape, along with their transportation and deposition zones (Frattini et al., 2004). Based on this information, a georeferenced database was generated for the purposes of the analyses discussed hereafter (5x5m DEM).

In addition, available rainfall intensity records from rain gauges located at nearby meteorological stations were used. Specifically, data from the Lauro station (i.e., the closest to the study area) were selected for the analyses.

3.2. Mechanical parameters

The model involves five mechanical parameters (Table 1). Among them, the first four parameters for Ash A were determined on the basis of standard geotechnical tests by Lizárraga and Buscarnera (2017). Slight variations in firction angle between ashes were reported by Pirone et al. (2015), while data for pumices is lacking. Thus, for simplicity, identical values of these parameters are here used for all layers. Finally, the remaining parameter r_w, which controls the susceptibility of a soil to wetting-induced instability, is back calculated for each layer based on the approach proposed by Lizárraga and Buscarnera (2017). Specifically, its value for the two ash is chosen to preserve the flowslide susceptibility calibrated by Lizárraga and Buscarnera (2017). By contrast, r_w is set to zero in the pumices, thus reflecting lack of flowslide triggering at depths corresponding to such layers.

3.3. Hydraulic parameters

The calibration of the hydrologic parameters for each layer is shown in Fig. 3. Correspondent data related to Water Retention Curve (WRC) and Hydraulic Conductivity Function (HCF) provided by Crosta and Dal Negro (2003) and Pirone et al. (2015) respectively. The model calibration results based on an exponential WRC (Stanier and Tarantino, 2010) and a Gardner HCF (Szymkiewicz, 2012) are displayed as continuous lines in Fig. 3. In addition, extensive tests regarding HCF of Ash A were conducted (Sorbino, 2005; Papa, 2007; Damiano et al., 2012), where the saturated permeability of such layer were reported between 1e-6 m/s and 3e-6 m/s.

4. Assessment of model performance

The proposed methodology is here tested against landslide records available for the city of Sarno, for which extensive field and laboratory data is available (Sorbino and Nicotera, 2013). Previous flowslide triggering simulations for this same site have been recently conducted with reference to uniform stratigraphic conditions (Lizárraga et al., 2017). As a consequence, the site offers a unique opportunity to compare the results obtained for the case of layered liquefiable slopes against those

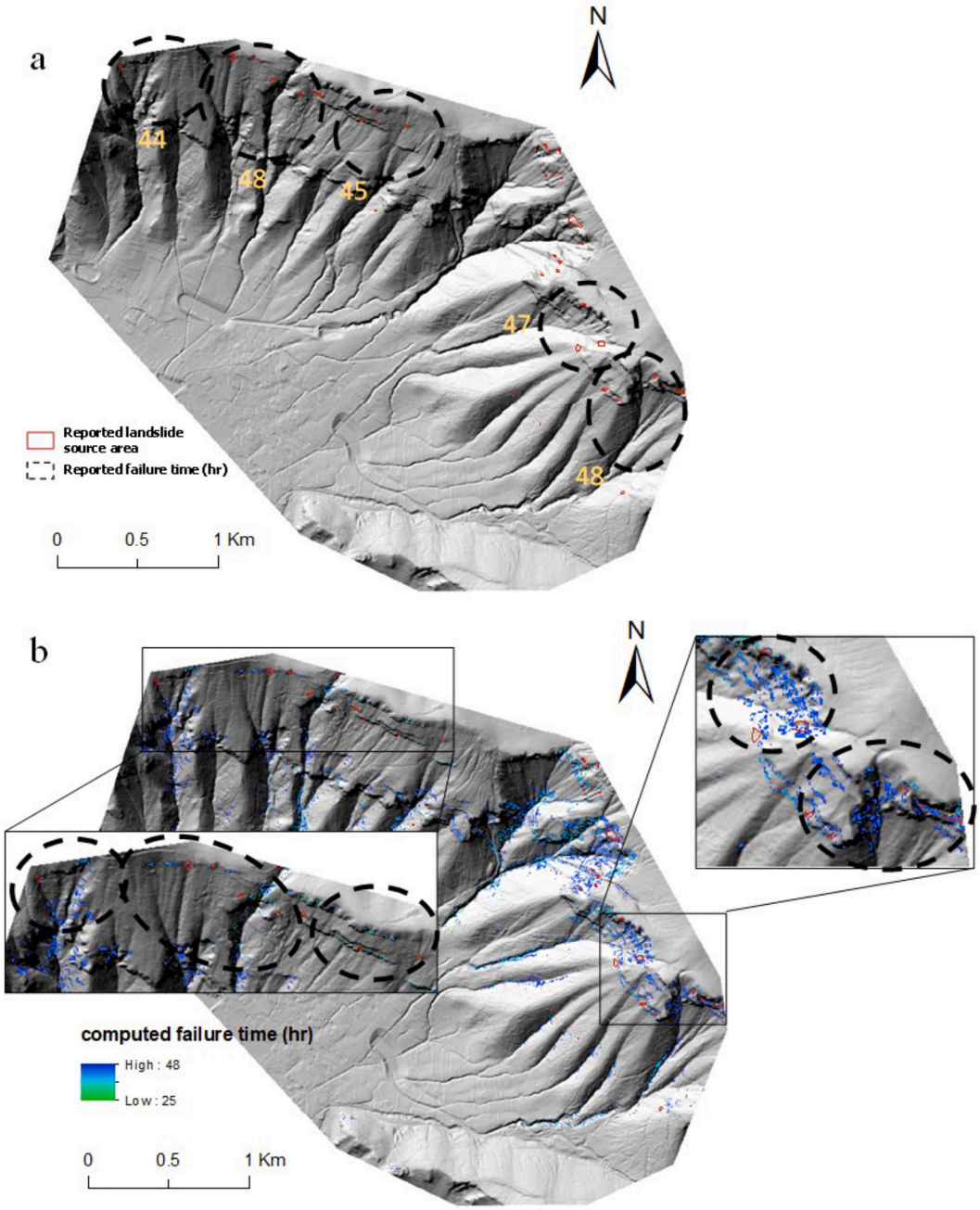

Fig. 8. Sarno landslide failure time a) reported from Cascini et al., 2011, b) calculated in this work.

resulting from the use of a baseline homogeneous model.

4.1. Categorization of failure mechanisms

Landslide types are often classified on the basis of their post-failure mobility. In this paper, the term *flowslide* is used to refer specifically to phenomena where static liquefaction is responsible for the initial triggering of the downslope movement, thus often resulting in rapid buildup of pore water pressure and consequent runaway failure of a fluidized soil mass (Hungr et al., 2014). This underlying mechanics is distinct from the phenomenology of frictional failure, in which a well-defined slip surface is generated and the failure leads to limited or negligible engagement of pore water pressure, as well as to relatively little mobility. For these reasons, this more common class of shallow failure is here referred to as *frictional slip*, in that it is treated as an uncoupled (drained) mechanism associated with the engagement the soil strength. Accordingly, the failure mechanisms detected at the Sarno site can be differentiated based on their propagation distance (Crosta and Dal Negro, 2003).

Let us consider for example area A in Fig. 4, where five landslides source areas were detected. Three of such landslides led to a post-failure movement of limited extent (i.e., runout distances lower than 30 m), and can thus be classified as frictional slips. On the contrary, the other two failures resulted into large downslope flow-like movements (i.e., runout distance larger than 1 Km), which propagated along the landscape gully. Such type of failures will be here categorized as flowslides. Although the analysis of the available data at the Sarno site indicates predominance of flow-like failure (i.e., 28% of frictional slips and 72% of flowslides), the distribution of failure mechanisms is by no means spatially homogeneous. In fact, sectors of the landscape where one type of failure mode is

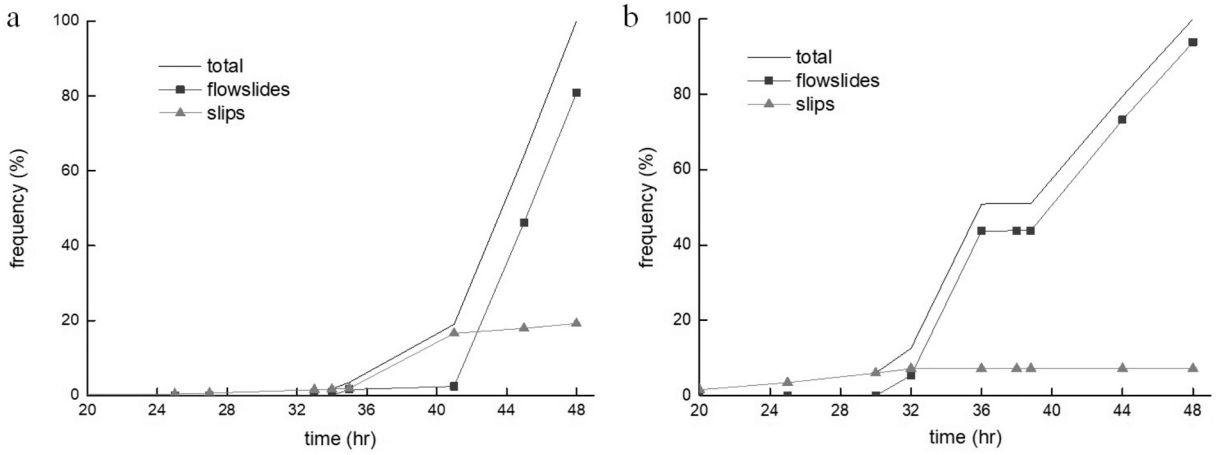

Fig. 9. Failure time history calculated from a). stratified model, b) homogeneous model.

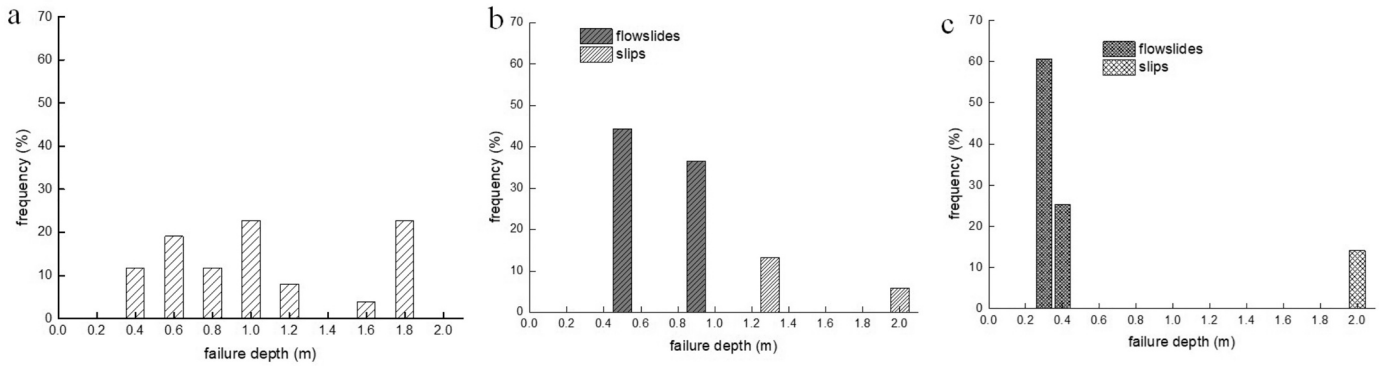

Fig. 10. Failure depth a) reported by Crosta and Dal Negro, 2003, b) calculated from the stratified model, c) calculated from the homogenous model.

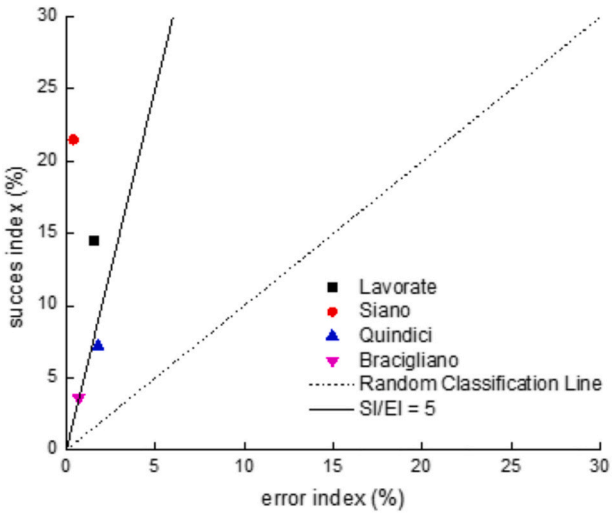

Fig. 11. Results of model spatial performance for four selected municipalities across the Pizzo d'Alvano massif.

predominant can be identified. This is the case of area B in Fig. 4, where a much higher concentration of frictional slips was detected compared to the rest of the site (9 slips out of total 12 failures). Such variations in the frequency of failure mechanisms will be used to test the spatial accuracy of the model predictions.

Preliminary analyses based on layered model slopes were conducted (see stratigraphic profile for the Sarno site in Fig. 2). Specifically, the simulations were inspected by comparing them with those of a homogeneous model based solely on the saturated permeability (k_s) of Ash A. For the latter, varying values of k_s equal to 1×10^{-6} m/s, 2×10^{-6} m/s and 3×10^{-6} m/s were used, in agreement with reported laboratory data. To ensure the consistency of the comparison, these values of k_s were also used to model Ash A in the stratified model. By contrast, the hydraulic properties of all other layers were set defined on the basis of the calibration in Fig. 3. Both models show satisfactory performance in capturing failure events spatial distribution (Fig. 6) when k_s equals to 2×10^{-6} m/s. (Details of computation results regarding spatial distributions are discussed in the next subsection, here the concentration is settled on the failure mechanisms.) Under this scenario, the failure mechanisms identified by the model are shown in Fig. 5.

The results show that the stratified model predicts the occurrence of 19% slips and 81% flowslides, while the homogeneous model computed only 8% slips. Therefore, although both models predict higher frequency of flowslides, the homogeneous case leads to a severe overestimation of flowslides, while the model based on a more realistic soil profile is characterized by a better agreement with the recorded landslide inventories.

The accuracy of the simulations can also be assessed in terms of its spatial accuracy. This is here done with reference to the previously mentioned area B (Fig. 6) in which frictional slips display higher concentration. It is readily apparent that the model with stratigraphic heterogeneity correctly predicts dominance of frictional slips in such sector, while the homogeneous model predicts almost exclusively the onset of flowslides. Such result further emphasizes the advantages resulting from a more realistic representation of permeability contrasts within

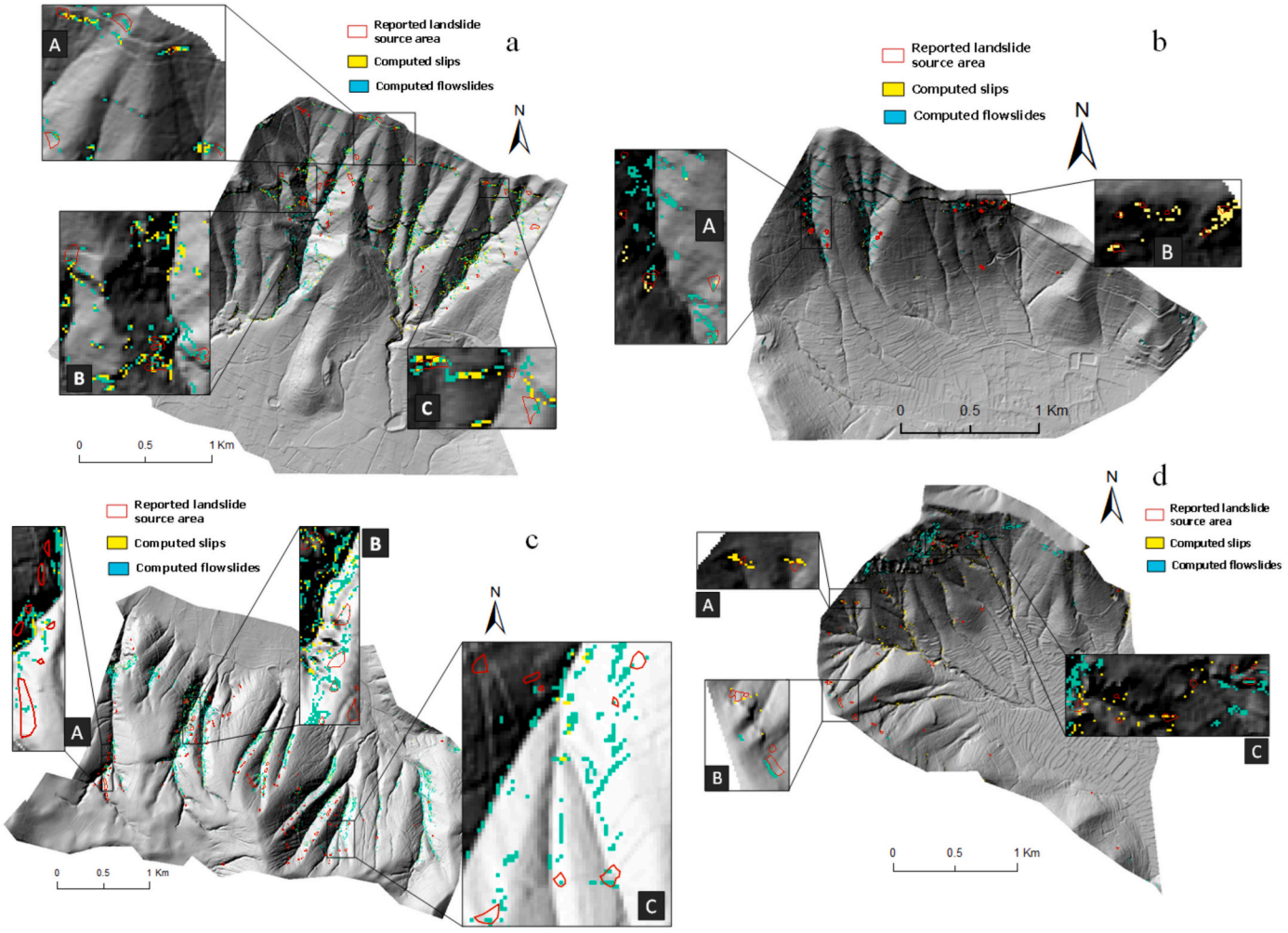

Fig. 12. Predicted failure triggering mechanisms at a) Lavorate, b) Siano, c) Quindici, d) Bracigliano.

naturally heterogeneous slopes.

4.2. Spatial performance

As discussed above, the simulation has been conducted with calibrated parameters (Table 1 & Fig. 3) and Ash A k_{sat} 1×10^{-6}, 2×10^{-6} and 3×10^{-6} m/s according to laboratory tests (Sorbino, 2005; Papa, 2007; Damiano et al., 2012). The results obtained through homogeneous and heterogeneous models are now compared in terms of Success Index (SI), Error Index (EI) and their ratio, SI/EI (Table 2). Such metrics proposed by Sorbino et al. (2010), can be used to assess quantitatively the model performance. In particular, SI represents the percentage ratio of computational cells indicated correctly the reported landslides sources, while EI illustrates the percentage of overprediction.

Results shown in Table 2, the optimized prediction of two models are both for K_s equals to 2×10^{-6} m/s scenarios. The performance of all models resulted in values of SI/EI ratio between 2 and 4 times larger than those reported in similar studies for this area. Although this signals a satisfactory performance of all model scenarios, the results based on a realistic depiction of the stratigraphic heterogeneity resulted into higher values of both SI and SI/EI compared to the corresponding homogeneous model. In other words, the incorporation of natural heterogeneity leads not only to better spatial accuracy, but also to more reliable identification of landslide source with lower overprediction of potentially unstable zones.

To further discuss the spatial performance of the model with layered slopes, Fig. 7 reports the landslide triggering susceptibility map obtained from simulations based on K_s of 2×10^{-6} for Ash A. Although certain sectors of the landscape are still characterized by overprediction (e.g., area D), the computations are able to identify all landslide source areas and the predominant type of slope failure. By contrast, in other sectors (e.g., areas A, B and C), satisfactory agreement with the reported landslide source areas is achieved with limited overprediction. In particular, four clusters of unstable cells were computed in area A, with three of them displaying considerable overlap with the reported source areas.

4.3. Temporal performance

The temporal stages of landslide initiation for part of the landslides that took place across the Sarno site (contours in Fig. 8a) was discussed by Cascini et al. (2011), who constrained the most likely failure times (44 to 48 h after the start of the rainstorm) on the basis of witness reports. Although the accuracy of such values is invariably affected by a number of uncertainties, it can be used as a tentative reference to assess the temporal performance of the model.

The computed failure time obtained from the model with layered slopes is shown in Fig. 8b for two specific areas. In the western sector of the landscape, the landslides enclosed by contours with bright green color represent earlier failure mobilization. Except the central contour, where failure was reported to have occurred at the end of the storm, these results are in good agreement with the data. In the eastern sector of the landscape, the computations are enclosed by contours with darker color, marking relatively late failure initiation. Such results are also consistent with the inventory, thus corroborating the accuracy of the

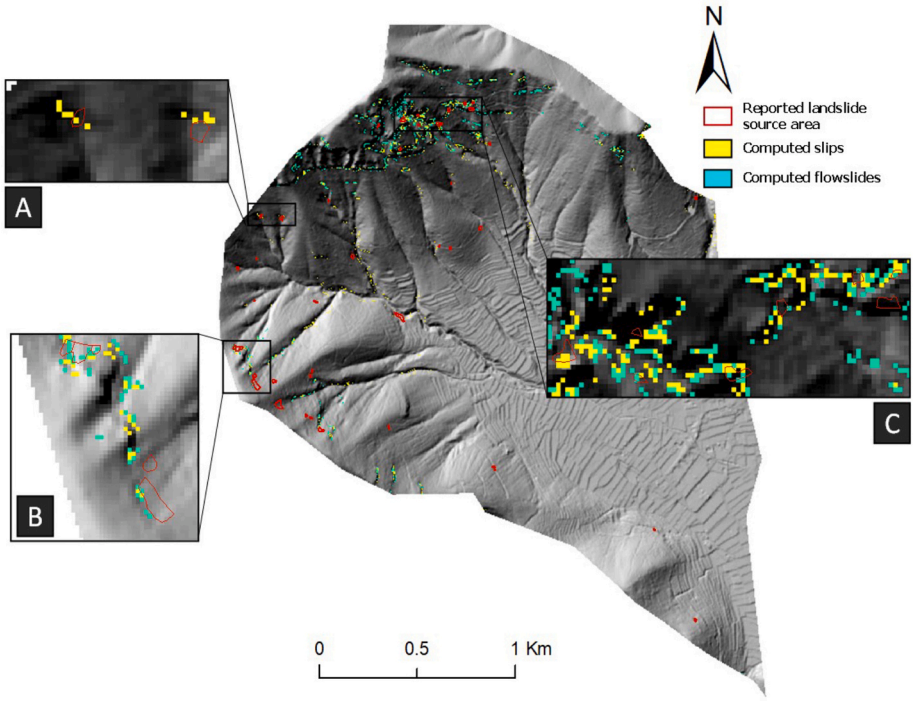

Fig. 13. Bracigliano failure distribution calculated by Siano stratification profile.

model performance also from the temporal standpoint.

At this reference, a further comparison between homogeneous and layered model is shown in Fig. 9. For both cases slips were predicted to have mostly occurred during the early stages of the storm. Most importantly, the reported failure time (Cascini et al., 2011) ranged between 44 and 48 h. From Fig. 9a it is readily apparent that the failures computed by the stratified model are concentrated after 41 h. By contrast, in the homogeneous model, the failure time distribution displays two peaks, one from 32 to 36 h, and another from 40 to 48 h. As a result, it can again be concluded that under the standpoint of the temporal predictions, the model based on stratified slopes provides a superior performance compared to an equivalent homogeneous model.

4.4. Failure depth

The failure depth is another important feature to assess the performance of a landslide modeling platform. Such feature can also be calculated both in the stratified and the homogenous model. The results are compared in Fig. 10 with reported data (based on which the failure depth ranges from 0.4 m to 1.8 m).

For both scenarios, flowslides tend to be obtained at shallow depths. However, while the homogeneous model predicts failure depths densely distributed around 0.4 m, the stratified model provides 40% failures at 0.5 m, 40% at 0.9 m, and 20% at depths deeper than 1.3 m. It is clear that the failure depths predicted by the stratified model resembles much more closely the distribution emerging from field surveys, thus indicating another important metric for which the incorporation of stratigraphic heterogeneity into a geomechanical model leads to beneficial outcomes.

5. Model application in other sites

Although, the richness of data at both field and laboratory scale, for the site of Sarno provides an optimal platform to test the model performance, here a broader set of validation examples are discussed with reference to four additional municipalities belonging to the same geological setting (Quindici, Lavorate, Siano and Bracigliano, Fig. 2). Such step relies on field surveys reported by Crosta & Dal Negro and Cascini & Sorbino, from which characteristic stratigraphic profiles for each of these sites were reported. As a result, this additional series of examples is functional to discuss the model performance in the presence of widely different vertical heterogeneity scenarios. Given the prevalence of alternations of deposits of Ash A, Ash B and pumices across Campania, the model functions and parameters previously discussed on the basis of data available for the Sarno site will be considered applicable also to this new set of analyses. This choice clearly represents a major simplification, in that rigorous analyses would require a complete reassessment of both site-specific hydraulic and mechanical properties, as well as initial and boundary conditions. However, despite its shortcomings, this choice is here simply intended as a working hypothesis aimed at testing differences in model performance for idealized cases in which variations of the stratigraphic profile represent the only important departure between one site and another.

Fig. 11 illustrates an assessment of the spatial performance of the model based on some of the metrics previously discussed, SI and SI/EI. The simulations for Quindici and Bracigliano return values of SI/EI between 3 and 5, hence much lower than those obtained for Sarno, but still close to previous model performances reported by other authors (Frattini et al., 2004; Sorbino et al., 2010; Godt et al., 2008). By contrast, the results reported in Lavorate is nearly twice has high (i.e., SI/EI = 9.3), and thus closer to the performance obtained for the Sarno site. Finally, an even superior performance was obtained with reference to the site of Siano, for which values of SI/EI nearly one order of magnitude higher that those obtained for the other sites were obtained (i.e., SI/EI = 54).

Such major variability in performance clearly suggests that, despite its importance, the stratigraphic profile cannot be regarded as the only factor differentiating one site from the other. At the same time, they indicate that the performance of all models relying on stratigraphic heterogeneity is at the very least comparable with that of other similar models available in the literature and can even be order of magnitudes superior to standard models when the calibrated parameters reflect the actual hydro-mechanics of the soils present at the site.

Fig. 12 displays the spatial performance of the model for each site.

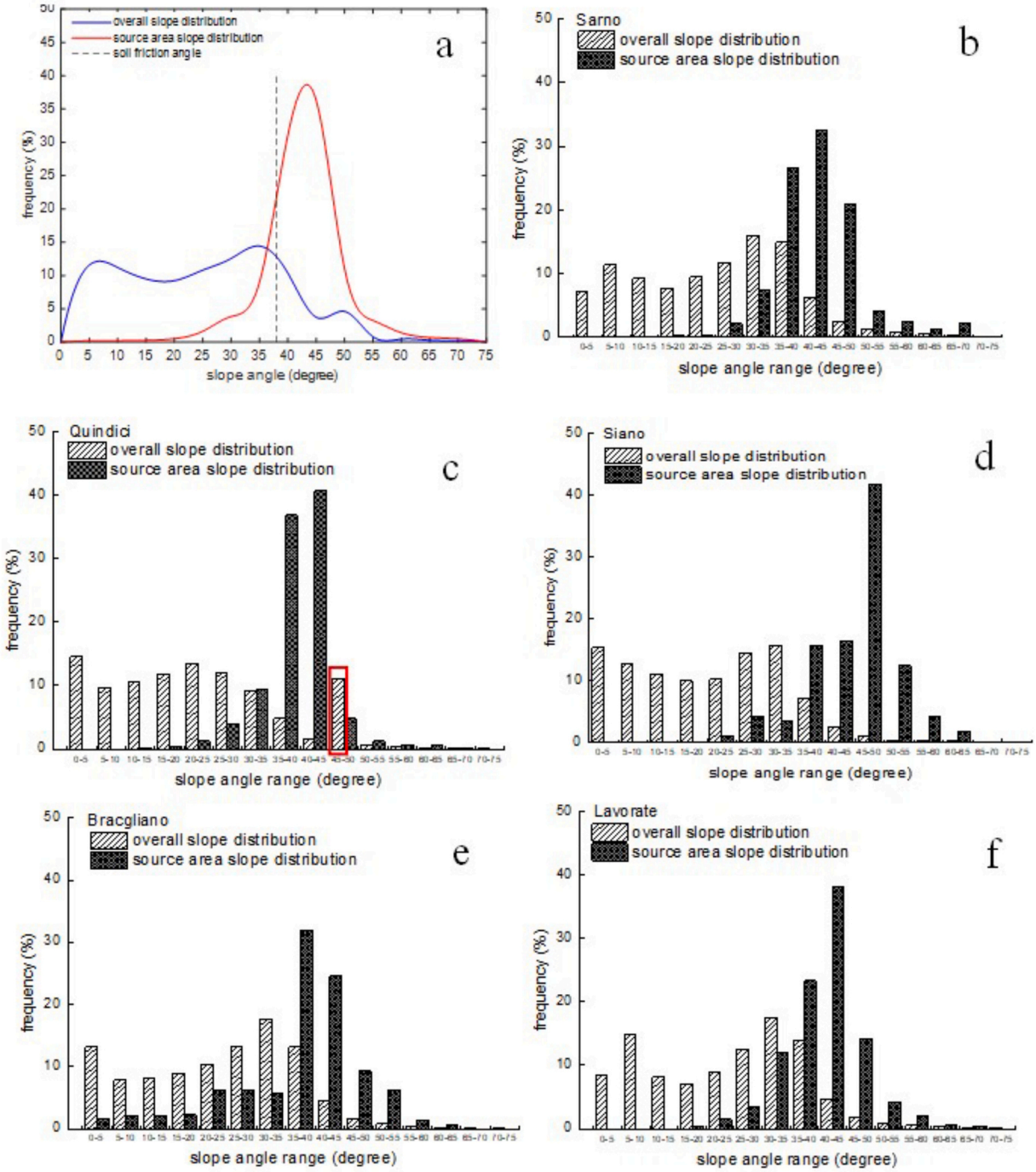

Fig. 14. Source area and landscape slope angle distribution for a) five studied municipalities, b). Sarno, c). Quindici, d) Siano, e) Bracgliano, f) Lavorate.

Specifically, in Lavorate (Fig. 12a), although few landslides in the northern sector are not captured, instability events were correctly identified at almost all other locations, especially in the areas labeled as A, B and C, where fourteen landslide contours show satisfactory overlap with the computed failure zones.

The results for the Siano site (Fig, 12b) also indicate an acceptable detection of source areas, while guaranteeing relatively low levels of overprediction. Specifically, in the areas labeled as A and B most failures are successfully captured.

Finally, as previously anticipated, the quality of the model performance cannot be regarded equally satisfactory for the sites Quindici and Bracgliano. With reference to Quindici, the source of this mismatch is highlighted in correspondence of the areas labeled as A, B and C (Fig. 12c), where the predictions simply surround the reported source areas instead of overlapping with them. Similar comments can be made for the Bracgliano site (Fig. 12d), where only few flowslides in the northern sector and scattered slips across the eastern part of the landscape have been predicted. Insets centered around the zones labeled as A, B and C correspondingly indicate that the reported failures are only partially captured.

6. Discussion

Despite the acceptable metrics obtained for all the five sites, such detailed analysis of the predicted spatial patterns of failure indicates remarkable variability of the model performance, thus requiring further

discussion. Specifically, it is necessary to explain the factors responsible for the relatively poor performance of the model at the sites of Quindici and Bracigliano, as well as identify possible future model refinements that could mitigate the current shortcomings.

Among the two abovementioned sites, the municipality of Bracigliano was modeled with a rather uniform soil profile based exclusively on Ash A (Fig. 2). Hence, the model lacked the highly permeable pumice layer characterizing the stratigraphic profile used for all the other sites. On one hand, this placed even further weight on the use of material properties calibrated for another site (i.e., Sarno), in that the use of a single layer would require a direct site-specific recalibration of the parameters associated with infiltration and failure. On the other hand, the assumption of perfect homogeneity may have led to relatively weaker pore pressure accumulation, which in other models was promoted by permeability contrasts and facilitated failure (see discussion in Lizárraga and Buscarnera, 2018). It is therefore possible that the complete removal of the pumice layer represents an oversimplification of the subsurface heterogeneity of the Bracigliano site, which, although less heterogeneous than others, may still have been impacted by the presence of pumices.

To test the latter argument, a further analysis was conducted with a layering based on the Siano stratigraphic profile (featuring a single pumice layer of 20 cm thickness). Such simulation leads to an improved spatial performance (SI = 10% and SI/EI = 12), as well as to a better match between computed and reported source areas (see highlighted areas A, B and C, in Fig. 13).

As for the municipality of Quindici, the model performance is heavily restricted by the relatively steep landscape morphology, across which few instability events were reported. Fig. 14a shows the slope angle of total source area of a near-Gaussian distribution with mean value around 45°.

In Quindici, more than 10% of the landscape is steeper than 45° (red polygon in Fig, 14c). However, most landslides took place at angles between 35° and 45°. This constitutes a challenge for spatially distributed triggering analyses. In fact, to capture a large percentage of source areas at this site, the model parameters should have triggering thresholds encompassing a sufficient set of hillslopes with inclination angles lower than 45°. If such were the case, however, the features of the Quindici landscape mentioned above will inevitably lead to major overprediction.

To provide further context, Fig. 14 compares the distribution of slope angles of all the inspected municipalities. Except Quindici, at all sites the landslide source areas display higher frequencies at steep angles compared with the distribution of inclinations for the rest of the landscape. This feature facilitates the optimization of a spatially distributed model based on topographic data, in that a triggering threshold distinguishing stable and unstable slopes is not likely to lead to major overprediction. This is not the case for Quindici, whose landscape morphology involves a large portion of steep slopes not reflected in the distribution of landslide source areas. This suggest that steep slopes at Quindici may benefit from not thoroughly identified local effects (e.g., root cohesion, undetected rock outcrops) which contribute to preserve their stability during the rainstorm. Hence, it is arguable that any improvement of the model performance at that particular site requires the incorporation of effects currently not included in the model, such as the role of vegetation, a more accurate mapping of rock outcrops, incorporation of water discharge from the bedrock, and use of spatially-distributed rainfall data.

7. Conclusions

This paper presented a regional-scale model to predict multi-modal shallow landslide initiation in stratified deposits. Emphasis was given to the distinction between two potential modes of failure, namely frictional slips of limited mobility and liquefaction-induced flowslides leading to runway failure. The framework is built around a vectorized Finite Element platform able to predict pore pressure transients in heterogeneous unsaturated soils slopes, while guaranteeing computational efficiency and versatile definition of material properties and initial/boundary conditions.

The model was tested against a series of shallow landslide events induced by heavy rainstorms for which extensive laboratory and field data were available. Comparisons between equivalent models with and without stratigraphic heterogeneity were shown, demonstrating that the incorporation of soil layering leads to an improvement of all the tested metrics of performance, ranging from the predicted proportion of different initiation mechanisms, the spatiotemporal accuracy of the results, and the computed depth of failure.

The model was then tested with reference to four additional municipalities located across the same geological setting, but characterized by widely different stratigraphic profiles. Although the performance of the model varied significantly from one site to another, in all cases the performance was at least comparable to that reported by similar regional-scale models available in the literature, while in other cases it led to a one-order of magnitude increase of the model success. As a result, the modeling platform proposed here can be regarded as a robust tool for landslide susceptibility zonation whenever information about site-specific stratigraphic heterogeneity is available.

Declaration of Competing Interest

With the present all the authors declare that they do not have any financial and/or personal conflict with other people or organizations that could inappropriately influence or bias their work.

Acknowledgements

This work was supported by Grant No. ICER-1854951 awarded by the U.S. National Science Foundation.

References

Ayalew, L., Yamagishi, H.J.G., 2005. The application of GIS-based logistic regression for landslide susceptibility mapping in the Kakuda-Yahiko Mountains, Central Japan. Geomorphology 65 (1–2), 15–31.

Baum, R.L., Coe, J.A., Godt, J.W., Harp, E.L., Reid, M.E., Savage, W.Z., Schulz, W.H., Berin, D.L., Chleborad, A.F., McKenna, J.P., Michael, J.A., 2005. Regional landslide-hazard assessment for Seattle, Washington, USA. Landslides. 2 (4), 266–279.

Baum, R.L., Godt, J.W., Savage, W.Z., 2010. Estimating the timing and location of shallow rainfall- induced landslides using a model for transient, unsaturated infiltration. Journal of Geophisical Research: Earth Surface 115, F3.

Bellugi, D., Milledge, D.G., Dietrich, W.E., McKean, J.A., Perron, J.T., Sudderth, E.B., Kazian, B. J. J. o. G. R. E. S., 2015. A spectral clustering search algorithm for predicting shallow landslide size and location. Journal of Geophisical Research: Earth Surface. 120 (2), 300–324.

Buscarnera, G., Di Prisco, C., 2011. Stability criteria for unsaturated shallow slopes. Int. J. Solids Struct. 1 (4), 85–90.

Buscarnera, G., Di Prisco, C., 2012. Discussing the definition of the second-order work for unsaturated soils. Int. J. Numer. Anal. Methods Geomech. 36 (1), 36–49.

Buscarnera, G., Di Prisco, C., 2013. Soil stability and flow slides in unsaturated shallow slopes: can saturation events trigger liquefaction processes. Géotechnique. 63 (10), 801–817.

Cascini, L., Sorbino, G., 2003. The contribution of soil suction measurements to the analysis of flowslide triggering. In: Paper presented at the Workshop "Flows".

Cascini, L., Cuomo, S., Sorbino, G., 2005. Flow-like mass movements in pyroclastic soils: remarks on the modelling of triggering mechanisms. Italian Geotechnical Journal 4, 11–31.

Cascini, L., Cuomo, S., Guida, D., 2008. Typical source areas of May 1998 flow-like mass movements in the Campania region, Southern Italy. Eng. Geol. 96 (3–4), 107–125.

Cascini, L., Cuomo, S., Della Sala, M., 2011. Spatial and temporal occurrence of rainfall-induced shallow landslides of flow type: a case of Sarno-Quindici, Italy. Geomorphology. 126 (1–2), 148–158.

Celia, M.A., Bouloutas, E.T., Zarba, R.L., 1990. A general mass-conservative numerical solution for the unsaturated flow equation. Water Resource Research. 26 (7), 1483–1496.

Chen, Z., Huan, G., Ma, Y., 2006. Computational methods for multiphase flows in porous media, vol. 2. Siam.

Crosta, G., Dal Negro, P., 2003. Observations and modelling of soil slip-debris flow initiation processes in pyroclastic deposits: the Sarno 1998 event. Natural Hazards and Earth System Science. 3 (1/2), 53–69.

Crosta, G., Frattini, P., 2003. Distributed modelling of shallow landslides triggered by intense rainfall. Natural Hazards and Earth System Science 3 (1/2), 81–93.
Cuomo, S., Iervolino, A., 2016. Investigating the role of stratigraphy in large-area physically-based analysis of December 1999 Cervinara shallow landslides. J. Mt. Sci. 13 (1), 104–115.
Damiano, E., Olivares, L., Picarelli, L., 2012. Steep-slope monitoring in unsaturated pyroclastic soils. Eng. Geol. 137, 1–12.
De Vita, P., Napolitano, E., Godt, J.W., Baum, R.L., 2013. Deterministic estimation of hydrological thresholds for shallow landslide initiation and slope stability models: case study from the Somma-Vesuvius area of southern Italy. Landslides. 10 (6), 713–728.
Di Crescenzo, G., Santo, A., 2005. Debris slides–rapid earth flows in the carbonate massifs of the Campania region (Southern Italy): morphological and morphometric data for evaluating triggering susceptibility. Geomorphology. 66 (1–4), 255–276.
Duncan, J.M., Wright, S.G., Brandon, T.L., 2014. Soil Strength and Slope Stability. John Wiley & Sons.
Frattini, P., Crosta, G.B., Fusi, N., Dal Negro, P., 2004. Shallow landslides in pyroclastic soils: a distributed modelling approach for hazard assessment. Eng. Geol. 73 (3–4), 277–295.
Godt, J.W., Baum, R.L., Savage, W.Z., Salciarini, D., Harp, E.L., 2008. Transient deterministic shallow landslide modelling: Requirements for susceptibility and hazard assessments in a GIS framework. Engineering Geology 102 (3–4), 214–226.
Guadagno, F., Forte, R., Revellino, P., Fiorillo, F., Focareta, M., 2005. Some aspects of the initiation of debris avalanches in the Campania Region: the role of morphological slope discontinuities and the development of failure. Geomorphology. 66 (1–4), 237–254.
Hungr, O., Leroueil, S., Picarelli, L., 2014. The Varnes classification of landslide types, an update. Landslides. 11 (2), 167–194.
Iverson, R.M., 2000. Landslide triggering by rainfall infiltration. Water Resour. Res. 36 (7), 1897–1910.
Iverson, R.M., 2005. Regulation of landslide motion by dilatancy and pore pressure feedback. Journal of Geophisical Research, v. 110.
Iverson, R.M., Major, J.J., 1987. Rainfall, ground-water flow and seasonal movement at Minor Creek landslide, Northwestern California: physical interpretation of empirical relations. Geological Society of America Bulletin. v. 99, 579–592.
Lizárraga, J., Buscarnera, G., 2017. Safety factors to detect flowslides and slips in unsaturated shallow slopes. Géotechnique. 68 (5), 442–450.
Lizárraga, J.J., Buscarnera, G.J.L., 2018. Spatially distributed modeling of rainfall-induced landslides in shallow layered slopes. Landslides. 16 (2), 253–263.
Lizárraga, J., Buscarnera, G., Frattini, P., Crosta, G., 2017. Spatially distributed modeling of landslide triggering: an approach based on principles of unsaturated soil plasticity. In: Landslides and Engineered Slopes. Experience, Theory and Practice. CRC Press, pp. 1287–1294.
McKenna, J.P., Santi, P.M., Amblard, X., Negri, J., 2012. Effects of soil-engineering properties on the failure mode of shallow landslides. Landslides. 9 (2), 215–228.
Montgomery, D.R., Dietrich, W.E., 1994. A physically based model for the topographic control on shallow landsliding. Water Resource Research. 30 (4), 1153–1171.
Pack, R.T., Tarboton, D.G., Goodwin, C.N., 1998. The SINMAP approach to terrain stability mapping. In: 8th Congress of the International Association of Engineering Geology. Vancouver, British Columbia, Canada.
Papa, R., 2007. Indagine sperimentale di una copertura piroclastica di un versante della Campania. PhD thesis. University of Naples.
Picarelli, L., Olivares, L., Avolio, B., 2008. Zoning for flowslide and debris flow in pyroclastic soils of Campania Region based on “infinite slope” analysis. Eng. Geol. 102 (3–4), 132–141.
Pirone, M., Papa, R., Nicotera, M.V., Urciuoli, G., 2015. In situ monitoring of the groundwater field in an unsaturated pyroclastic slope for slope stability evaluation. Landslides. 12 (2), 259–276.
Reid, M., 1997. Slope instability caused by small variations in hydraulic conductivity. J. Geotech. Geoenviron. 123 (8), 717–725.
Richards, L.A., 1931. Capillary conduction of liquids through porous mediums. Physics. 1 (5), 318–333.
Sorbino, G., 2005. Numerical Modelling of Soil Suction Measurements in Pyroclastic Soils. Int. Symp.“Advanced Experimental Unsaturated Soil Mechanics”. Taylor and Francis Group, London.
Sorbino, G., Nicotera, M.V., 2013. Unsaturated soil mechanics in rainfall-induced flow landslides. Eng. Geol. 165, 105–132.
Sorbino, G., Sica, C., Cascini, L., 2010. Susceptibility analysis of shallow landslides source areas using physically based models. Nat. Hazards 53 (2), 313–332.
Srivastava, R., Yeh, T.C.J., 1991. Analytical solutions for one-dimensional, transient infiltration toward the water table in homogeneous and layered soils. Water Resour. Res. 27 (5), 313–332.
Stanier, A., Tarantino, A., 2010. Active earth force in ‘cohesionless’ unsaturated soils using bound theorems of plasticity. In: Proceedings Proc. of 5th Int. conf. on Unsaturated Soils, Barcelona, pp. 1081–1086.
Szymkiewicz, A., 2012. Modelling Water Flow in Unsaturated Porous Media: Accounting for Nonlinear Permeability and Material Heterogeneity. Springer Science & Business Media.
Van Dam, J., Feddes, R.A., 2000. Numerical simulation of infiltration, evaporation and shallow groundwater levels with the Richards equation. J. Hydrol. 233 (1–4), 72–85.
Van Westen, C., Van Asch, T.W., Soeters, R., 2006. Landslide hazard and risk zonation—why is it still so difficult? Bulletin of Engineering Geology and Environment. 65 (2), 167–184.
Wu, W., Sidle, R.C., 1995. A distributed slope stability model for steep forested basins. Water Resource Research. 31 (8), 2097–2110.
Zienkiewicz, O.C., Chan, A., Pastor, M., Schrefler, B., Shiomi, T., 1999. Computational Geomechanics. Citeseer.